Stability, structural, and electronic properties of atomic chains on Yb/Ge(111)3×2 studied by STM and STS

M. Kuzmin,[1,2,*] P. Laukkanen,[1,3] R. E. Perälä,[1] M. P. J. Punkkinen,[1,4] M. Ahola-Tuomi,[1] J. Lång,[1] and I. J. Väyrynen[1]

[1]*Department of Physics and Astronomy, University of Turku, FI-20014 Turku, Finland*

[2]*Ioffe Physical-Technical Institute, Russian Academy of Sciences, St. Petersburg 194021, Russian Federation*

[3]*Optoelectronics Research Centre, Tampere University of Technology, FI-33101 Tampere, Finland*

[4]*Applied Materials Physics, Department of Materials Science and Engineering, Royal Institute of Technology, SE-10044 Stockholm, Sweden*

(Received 24 September 2009; revised manuscript received 16 March 2010; published 15 April 2010)

By means of scanning tunneling microscopy and spectroscopy (STM/STS), we have investigated the stability and the structure of atomic chains on Yb/Ge(111)3×2. STM allows the identification of different building blocks of this reconstruction, depending on the bias polarity and voltage, and validates the honeycomb chain-channel (HCC) structure with the Ge=Ge double bond and metal coverage of 1/6 ML for Yb/Ge(111)3×2, in agreement with the recent photoemission study [Kuzmin *et al.*, Phys. Rev. B **75**, 165305 (2007)]. The Yb atoms are found to be adsorbed on similar sites in the well-defined ×2 rows. Locally, such rows are distorted, leading to the ×4 periodicity, where the Yb atoms are adsorbed on two different sites that are well consistent with T4 and H3 sites. It is also assumed that Yb atoms can fluctuate rapidly between the neighboring T4 and H3 sites, leading to continuous rows observed together with the ×2 rows in STM images. The stability of Ge honeycomb chain is controlled by the presence of Yb atom per two (3×1) surface units in average, which results in the donation of one electron from Yb to the surface per (3×1) unit. When this density is locally changed, the Ge honeycomb chain is found to be broken. The inner structure of the Ge honeycomb chain is visualized in STM and shows dimerized features without any apparent buckling. The STM observations also account for why the double periodicity is missing in the low-energy electron diffraction pattern from Yb/Ge(111)3×2. The local electronic structure of this reconstruction, namely the Yb rows and Ge honeycomb chains, is studied by STS. The results support the HCC structure with the Ge=Ge double bond. It is believed that the present study elucidates the difference between the (3×2) reconstructions of Yb and Eu on Ge(111) and those of alkaline-earth and rare-earth metals on Si(111).

DOI: 10.1103/PhysRevB.81.155312 PACS number(s): 68.35.Ct, 68.37.Ef, 68.43.Fg, 73.20.At

I. INTRODUCTION

Metal-induced reconstructions of semiconductor surfaces have been the subject of various studies due to both fundamental and technological importance of these systems for more than three decades.[1] From the fundamental point of view, these reconstructions can act as a model system to investigate many surface phenomena, such as the adsorption, growth, and catalysis, as well as the relation of structural, electronic, and chemical properties of an interface.

The $(3\times n)$ reconstruction induced on Si(111) by monovalent ($n=1$) and divalent ($n=2$) metal atoms ranging from Ag and alkali metals (AM) to alkaline earths and rare earths (AE and RE, respectively) (Refs. 2–17) is one of the striking examples illustrating how the structure of the metal-adsorbed semiconductor surface is stabilized by the donation of electron charge transferred from the adsorbate atoms to the substrate such that the half-occupied orbitals are fully eliminated leading to the semiconducting band structure. The atomic arrangement of metal/Si(111)3×n has been well understood in terms of the so-called honeycomb chain-channel (HCC) model.[5–7] Figure 1 depicts three variants of the HCC model, namely, the (3×1) structure with 1/3 monolayer (ML) of monovalent metal atoms at the T4 adsorption sites [Fig. 1(a)] and (3×2) structures with 1/6 ML of divalent metal atoms at T4 [Fig. 1(b)] or H3 [Fig. 1(c)] sites [hereafter (3×1)-T4, (3×2)-T4, and (3×2)-H3, respectively]. In all these models, the topmost silicon atoms [i.e., *a*-*d* in Fig. 1(a), *a*-*d* and *a*′ in Fig. 1(b), and *a*-*d* and *d*′ in Fig. 1(c)] form almost planar honeycomb chains separated by the channels that adopt the metal atoms. The stability of the HCC structure for different adsorbates and their coverages is controlled by the electron counting rule according to which the HCC geometry requires the donation of one electron from the adsorbate atoms to the substrate per (3×1) surface unit irrespective of the adsorbed species.[16,17] Thus, the stabilization of HCC on Si(111) can occur either at 1/3 ML of monovalent atoms [Fig. 1(a)] or at 1/6 ML of divalent atoms, leading to the (3×1) and (3×2) periodicities, respectively. It is essential that trivalent metal adsorbates (such as Dy, Ho, Er, and Gd) form neither (3×1) nor (3×2) HCC reconstruction, in good agreement with the above rule; instead they give rise to a (5×2) structure consisting of honeycomb and Seiwatz chains of silicon atoms, which obeys the electron counting picture leading to a semiconducting surface band structure (Ref. 18 and references therein). In addition, an unusual Si=Si double bond formed by the silicon atoms *b* and *c* in the models of Fig. 1 is another stabilizing influence of the HCC structure.[6]

Since germanium is a group IV element like silicon, similar reconstructions can be expected for isoelectronic metal/Ge(111) and —Si(111) surfaces. Indeed, based on the surface x-ray diffraction and low-energy electron-diffraction (LEED) *I*-*V* measurements, it has been shown that Na—,

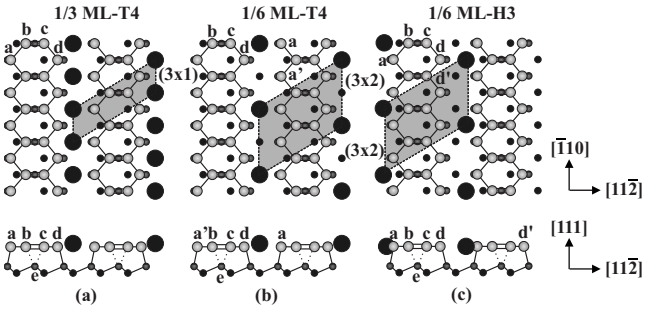

FIG. 1. HCC structures of the Si(111)(3×1) and -(3×2) surfaces with monovalent and divalent metal adsorbates, respectively. (a) The (3×1) structure with the 1/3 ML coverage of monovalent atoms adsorbed at the T4 sites. [(b) and (c)] The (3×2) structures with the 1/6 ML coverage of divalent atoms adsorbed at T4 and H3 sites, respectively. The metal atoms are represented by large solid circles. The (3×1) and (3×2) unit cells are shown by shadowed parallelograms.

Li/Si(111)(3×1), and Rb/Ge(111)(3×1) have similar bonding configurations.[5] More recently, utilizing scanning tunneling microscopy (STM),[19,20] angle-resolved ultraviolet photoelectron spectroscopy,[21] core-level spectroscopy,[21,22] transmission electron measurements,[23] and density-functional theory (DFT) calculations,[24] the Ge(111)(3×1) reconstructions stabilized by monovalent metals [Ag and AM (Li, Na, and K)] have been interpreted, in general, with the HCC geometry in Fig. 1(a). It has, however, remained unresolved whether the Ge=Ge double bond, similar to the Si=Si double bond, is present on the Ge HCC surface. No evidence for the antibonding π^* state originating from the Ge=Ge has been found in the STM images from Na/Ge(111)(3×1).[19,25] Moreover, recent DFT calculations in Ref. 21 showed that the Ge double bond does not exist on Li/Ge(111)(3×1) and that at this surface the atoms *b* and *c* are located asymmetrically relative to the atom *e* [see Fig. 1(a)]. Meanwhile, in the other theoretical study (Ref. 24), the buckled (nonplanar) HCC configuration of AM/Ge(111)(3×1) has not been found to be stable, whereas the flat arrangement with the Ge(*b*)=Ge(*c*) double bond was favorable, contrary to the results of Ref. 21. Also, the double bond between *b* and *c* in the Li/Ge(111)(3×1) has been confirmed by STM in Refs. 19 and 20. To recapitulate, the existence of the Ge=Ge double bond has still remained far from being resolved for the (3×1) HCC reconstructions.

Recently, we reported on two related systems, Eu/Ge(111) (Refs. 26 and 27) and Yb/Ge(111) (Ref. 28) that belong to the family of the (3×*n*) HCC reconstructions. Using STM it was demonstrated that Eu on Ge(111) at 1/6 ML forms a structure which is similar to those of AE— and RE/Si(111)(3×2).[26] However, in addition to the (3×2) periodicity, the Eu/Ge(111) was found to feature a local (3×4) periodicity, hitherto not reported for the case of Si; it was interpreted to exist due to the Eu atoms adsorbed on two nonequivalent sites in channels of the HCC Ge substrate. Based on core-level data, a modified HCC model was also proposed for the Yb/Ge(111)3×2 in Ref. 28, where a buckled Ge(*b*)=Ge(*c*) bond served as a novel structural element. In this study, we address the atomic and electronic structure

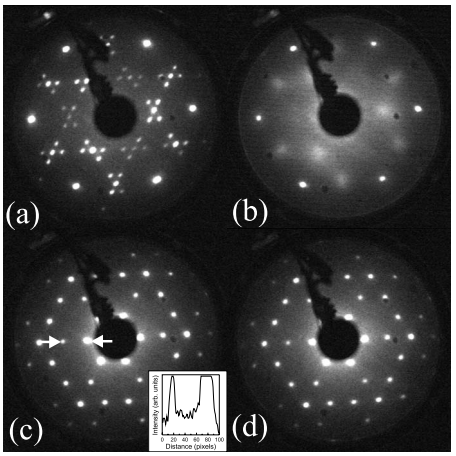

FIG. 2. (a) LEED pattern for the clean Ge(111)*c*(2×8) surface. (b) LEED pattern for the Yb overlayer grown on Ge(111)*c*(2×8) at room temperature. The coverage is 0.17 ML. [(c) and (d)] LEED patterns for the Yb/Ge(111)3×2 surface at 0.17 ML after annealing at 400 °C. The patterns were captured at room temperature and 400 °C, respectively. The electron energy is [(a) and (b)] 29 eV and [(c) and (d)] 37 eV. The inset of (c) shows the intensity profile taken along the line shown by arrows in the LEED pattern.

of Yb/Ge(111)3×2 by utilizing STM and scanning tunneling spectroscopy (STS). In particular, the existence and possible buckling of the Ge=Ge double bond, and the stability and properties of atomic chains on this surface are examined. We show bias-dependent STM images which clearly support the HCC geometry with the Ge=Ge double bond. However, no evidence is found that the Ge=Ge is essentially buckled. The structure of Yb rows and the location of metal atoms in such rows (i.e., the number of adsorption sites) are thoroughly discussed. These data clarify the findings for the Yb— and Eu/Ge(111)(3×2) reconstructions, according to which no half-order features are seen from these surfaces in LEED (Refs. 26–28). The local electronic structure of Yb/Ge(111)3×2 studied by STS is also found to be consistent with the HCC structure.

II. EXPERIMENTAL

The measurements were performed in the ultrahigh vacuum system with the base pressure below 1×10^{-10} mbar. The system was equipped with Omicron STM, LEED, x-ray photoelectron spectroscopy (XPS), and ion bombardment facilities. The Ge samples were cut from an Sb doped (*n*-type) (111) wafers (M.T.I. Corporation). Sample cleaning was carried out by repeated cycles of 700 eV Ar^+ sputtering at 400 °C and subsequent annealing at 620 °C until an excellent *c*(2×8) LEED pattern with sharp fractional-order spots and a low background [Fig. 2(a)] was found. STM images taken from the clean surface indicated that the *c*(2×8) structure is added by small portions of (2×2) and *c*(2×4) structures. XPS showed no carbon and oxygen related contaminations. The sample heating was performed by a direct current. The temperature was measured by an infrared pyrometer.

Ytterbium was deposited from a tungsten filament evaporator. The deposition rate was determined by a quartz-crystal microbalance and in addition it was verified by monitoring a series of (3×2), (5×1), (7×1), and (2×1) LEED patterns from the Yb/Si(111) surface as function of deposition time (Ref. 12). One monolayer of Yb on Ge(111) was referred to as the atomic density of the bulk-terminated surface (7.22×10^{14} atoms/cm^2). During the metal deposition the Ge substrate was held at room temperature (RT), resulting in a gradual disappearing of the $c(2\times8)$ LEED pattern with increasing the quantity of metal atoms (without subsequent annealing). In particular, only weak diffuse $c(2\times8)$ spots were observed at 1/6 ML, whereas the (1×1) spots remained almost as sharp and bright as for the clean surface, as shown in Fig. 2(b). The (3×2) reconstruction was produced by subsequent annealing of Yb overlayers on Ge(111) at 300–400 °C for 3–20 min. The variation in Yb coverage in the 0.10–0.17 ML range resulted in changing the ratio of bare and metal-covered surface areas. The surface was entirely covered with the Yb-induced (3×2) reconstruction at 0.17 ML where bright (3×1) LEED spots were observed without any sign of $c(2\times8)$ spots at both RT [Fig. 2(c)] and 400 °C [Fig. 2(d)] directly. No half-order spots and streaks were found at various electron energies, as illustrated in the inset of Fig. 2(c) that depicts the intensity profile taken along the line between the neighboring fractional-order spots of the (3×1) LEED pattern [shown by arrows in Fig. 2(c)]. This is consistent with the previous LEED observations for Yb—(Ref. 28) and Eu/Ge(111)(3×2) (Refs. 26 and 27) but not with those of RE/Si(111)(3×2) that clearly showed 1/2-order streaks or/and spots superimposed on the (3×1) pattern (Refs. 12–14 and 29). The STM and STS measurements were carried out at RT. The STM images were taken in the constant current mode. The tunneling spectra were acquired by using the current imaging tunneling spectroscopy (CITS) mode, where a series of tunnel current images was obtained at different bias voltages (which were constant for each image) and a topography image was also measured simultaneously. The WSXM package[30] is partially used for processing the STM and STS data.

III. RESULTS AND DISCUSSION

A. STM

Figure 3 shows filled state STM images measured for Yb/Ge(111)3×2 at various sample bias voltages (V_S). In Fig. 3(a), the image taken at $V_S=-2.23$ V shows up double rows of protrusions running in the $[\bar{1}10]$ direction. As seen in the inset of this image, a high-resolution filled state image taken with high magnification clearly demonstrates that the maxima of double rows are arranged in zigzag chains, which is the well-established fingerprint of the HCC structure (Ref. 6). In such images the protrusions are contributed by the dangling-bond states caused by the outer atoms of the honeycomb chains [i.e., a and d in Fig. 1(a), a, d, and a' in Fig. 1(b), and a, d, and d' in Fig. 1(c)]. The distance between the neighboring zigzag chain features in the $[11\bar{2}]$ direction is $(\sqrt{3}/2)\cdot3a_0$, where $a_0=4.0$ Å is the unit length on

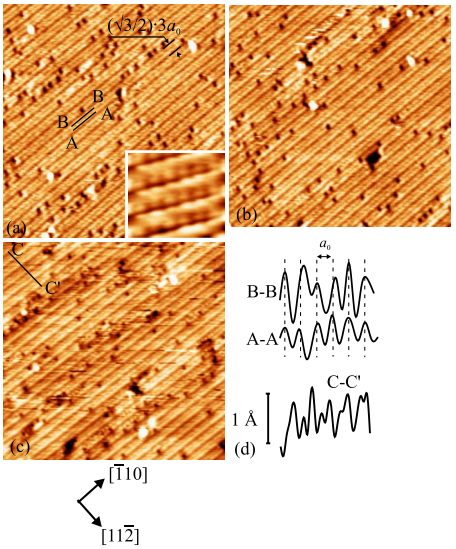

FIG. 3. (Color online) Bias-dependent STM images for the Yb/Ge(111)3×2 reconstruction in the filled states. The bias voltage V_S is (a) −2.32 V, (b) −1.70 V, and (c) −1.08 V. The tunneling current is (a) 69, (b) 56, and (c) 42 pA. The inset of (a) shows a high-resolution image of zigzag chain features (4.2 nm $\times$3.7 nm). (d) The line profiles A-A, B-B, and C-C′ taken along and across the zigzag chains in (a) and (c). The vertical bar shows the scale along the [111] direction.

Ge(111)(1×1). As shown in Fig. 3(d), the line profiles A-A and B-B taken along the two adjacent rows of the zigzag chain feature in Fig. 3(a) indicate that the distance between the neighboring protrusions in a row is basically a_0, that is, the zigzag chains have a single periodicity in the $[\bar{1}10]$ direction. A closer inspection, however, reveals that the zigzag chain features are locally slightly distorted; in particular, the neighboring protrusions tend to be grouped in pairs. Especially, the $\times2$ pairing effect is observed for the line profile B-B. Thus, the zigzag chain features locally show the $\times2$ periodicity along a chain. Earlier, a similar behavior has been reported for divalent metals, Ba,[9] Ca,[31] and Sm (Ref. 10) on Si(111), and Eu (Ref. 26) on Ge(111), and also supported by calculations in Refs. 9, 15, and 32. This effect is explained by the electrostatic interaction between the metal ion and the neighboring honeycomb atoms [e.g., d in the 3×2-T4 structure of Fig. 1(b)], leading to slight displacement of both d atoms to each other and the doubling of periodicity along the honeycomb chain.[9] Whereas the distortion along the other outer row of the honeycomb chain [i.e., along the row composed of the atoms a and a' in Fig. 1(b)] is much more hardly recognized. Obviously, the filled state STM data for the Yb/Ge(111)3×2 support well the above scenario and thus they are consistent with the HCC structure of the Ge substrate, which is locally distorted by the $\times2$ pairing effect.

The further analysis of STM data in Fig. 3 shows that the filled state images of Yb/Ge(111)3×2 are bias dependent, which is not reported for related systems before. As seen in Fig. 3(b), the adjacent rows of zigzag chains locally have a contrast in brightness at $V_S=-1.70$ V. This difference becomes more pronounced at −1.08 V [Fig. 3(c)]. As depicted in Fig. 3(d), the line profile C-C′ taken across zigzag chains

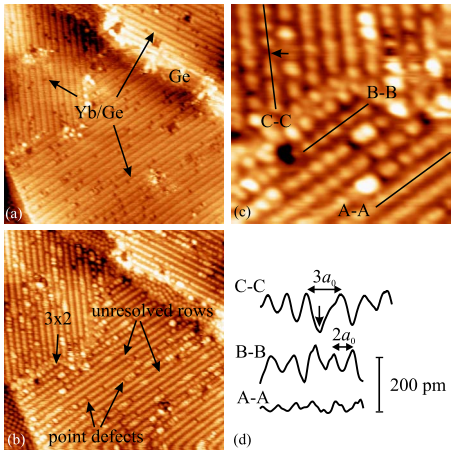

FIG. 4. (Color online) [(a) and (b)] Filled and empty state STM images of almost the same surface area on Yb/Ge(111)3×2. The bias voltages are −2.32 and +2.32 V, respectively. The tunneling current is 106 pA. (c) A high-resolution empty state (V_S= +2.32 V and I_t=106 pA) STM image with larger magnification. (d) Line profiles A-A, B-B, and C-C. The vertical bar shows the scale along the [111] direction.

in Fig. 3(c) reveals the noticeable difference in height level of the adjacent rows of zigzag chains. One can readily expect that the bonding configurations and charge states of the outer Ge honeycomb atoms in the HCC structure are not identical. For example, in Fig. 1(b) the metal atom is surrounded by the two nearest-neighbor atoms *d*; it also faces the atom *a* and does not interact directly with the atom *a*′. Thus, the contrast in height level of the adjacent rows of the zigzag chain is thought to reflect most likely the difference in charge distribution for the outer Ge honeycomb atoms. Also, the Yb atoms can slightly move toward the row of *d* atoms in the (3×2)-T4 or *a* atoms in the (3×2)-H3, leading to an increase in the valence charge of these atoms. This rearrangement is possible because the shift of Yb atoms would facilitate a larger angle between the two bonds of the Yb atom and the two neighboring Ge atoms. For more detailed analysis, however, calculations are needed.

Another prominent quality of the images in Fig. 3 is the abundance of defects that appear as dark depressions along the zigzag chains. It is essential that such defects are distributed nonuniformly. We found that about 68% of the defects appear on the brighter row of the zigzag chain. The origin of such propensity is still unclear. We notice that a similar behavior has been reported for filled state STM images of Li/Ge(111)(3×1), where the defects are distributed along one of the two adjacent rows of the zigzag chain feature.[20] For Yb/Ge(111)3×2, the defects can originate from a local distortion of metal rows in the HCC channels or/and contaminations. For example, STM images from Au/Si(553) (Ref. 33) and Au/Si(111)(5×2) (Ref. 34) and have been found to show similar defects caused by the adsorption of water molecules. We will discuss the origin of defects of Fig. 3 in more detail below.

The left panel of Fig. 4 shows STM images taken from almost the same surface area (not simultaneously) in both filled and empty states (V_S=−2.32 and +2.32 V, respectively). Three equivalent domains of the (3×2) reconstruction, which are rotated by 120°, along with a small bare Ge region are seen in these images. As described above, the filled state image [Fig. 4(a)] exhibits the double rows with zigzag chain features. In empty states [Fig. 4(b)], the surface shows up single rows of protrusions, where the distance between these rows is $(\sqrt{3}/2)\cdot 3a_0$. Frequently, the protrusions in a row are clearly resolved and have the $2a_0$ separation, leading to the well-defined ×2 periodicity along a row. However, such rows have a local character. First, a poor resolution can be locally found along the rows, leading to continuous segments in Fig. 4(b). Figure 4(c) represents a zoom in of the image in Fig. 4(b), where the line profiles are taken along the continuous and well-resolved ×2 rows (A-A and B-B, respectively). Comparison of these curves reveals that the rows have a similar periodicity, which is ×2, but very different height contrast.

Second, the regularity of ×2 rows is locally broken by point defects (vacancies) appearing as dark depressions marked by arrows in Fig. 4(b). The line profile C-C taken along a row with the point defect in Fig. 4(c) is depicted in Fig. 4(d). It shows that the separation of the protrusions adjacent to the point defect is $3a_0$, whereas the separation of other protrusions in this row is not affected by this defect and equal to $2a_0$.

Third, the well-resolved ×2 rows can locally exhibit nonequivalent protrusions. In Fig. 5(a), the row D-D′ includes a protrusion of which location is not identical to those of other protrusions. The line profile D-D′ shown in Fig. 5(c) reveals that the distances between this protrusion and the two neighboring maxima in a row are $2.5a_0$ and $1.5a_0$. For comparison, the row E-E′ has the regular corrugation with the 2× periodicity. Moreover, the presence of two nonequivalent protrusions can locally lead to the ×4 periodicity, as shown by the line profile F-F′ in Fig. 5(b).

Assuming that the protrusions of Yb-stabilized domains in the empty state images of Figs. 4 and 5 are centered on metal atoms,[6] we discuss here the atomic arrangement of the rows considered above. The identical positions of protrusions in the well-defined ×2 rows suggest that the Yb atoms reside at equivalent sites in such rows. According to *ab initio* calculations in Refs. 9, 24, and 32, the most favorable sites for metal atoms in the HCC structure on both Si(111) and Ge(111) are T4 and H3, and the energy difference between them is very small. In Fig. 6(a), the arrangement of the ×2 row with Yb atoms adsorbed on T4 sites in the channel of the HCC structure is shown. Note that this arrangement is identical to that of metal rows in the (3×2)-T4 model shown in Fig. 1(b). The ×2 row in Fig. 6(a) suggests that every second T4 site is unoccupied. When the two neighboring T4 sites are unoccupied [shown by arrows in Fig. 6(b)] and thus the ×2 row is distorted, it is expected that dark depression appears in the ×2 row, which is consistent with STM images in Fig. 4, where the ×2 rows with point defects are present. It is essential that the regular ×2 periodicity of such rows is observed out the point defect, as found in Fig. 4(c). That is, the point defect leads to the shift of ×2 Yb row by a_0. Therefore, it is unlikely that the point defects are due to contamination atop the intact ×2 row. Since the location of point defects in empty state image [Fig. 4(b)] coincides with the location of

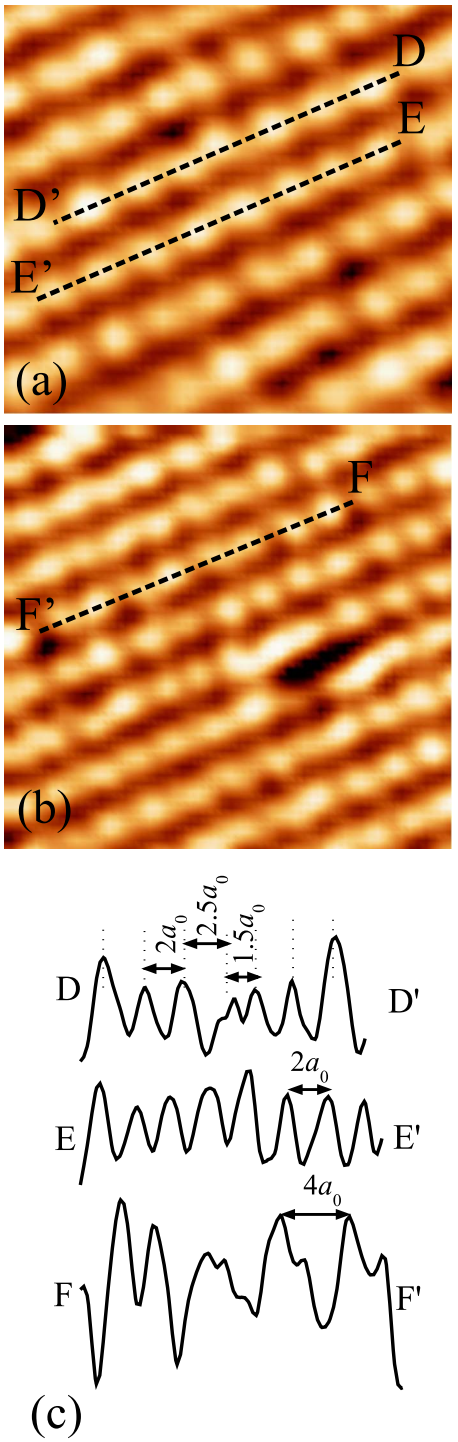

FIG. 5. (Color online) [(a) and (b)] High-resolution empty state STM images of Yb/Ge(111)3×2. The bias voltage is +2.04 V. The tunneling current is 80 pA. (c) Line profiles D-D′, E-E′, and F-F′.

dark depressions in filled state one [Fig. 4(a)], we suggest that these defects influence the Ge HCC structure [e.g., the atoms d', a', and a'' in Fig. 6(b)]. Indeed, an appearing of the point defect leads to the violation of the electron counting rule, which is required to stabilize the HCC structure, in the vicinity of this defect. Therefore, the HCC structure can be locally modified or destroyed. Note that in Fig. 6(b) no

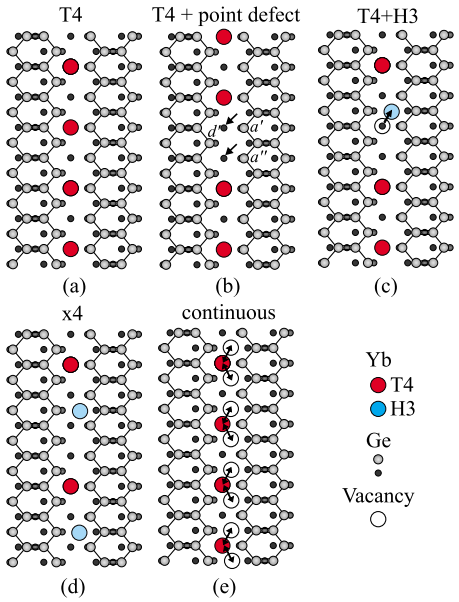

FIG. 6. (Color online) Atomic models of Yb rows observed in empty state STM images of Figs. 4 and 5. For details see the text.

modification the HCC structure is shown for the sake of simplicity.

In Figs. 6(c) and 6(d), we suggest models that explain the line profiles D-D′ and F-F′ in Fig. 5. Shown in Fig. 6(c) is the ×2 row distorted by a shift of Yb atom from the T4 to the neighboring H3 site, which is well consistent with the line profile D-D′. In fact, the distances between the Yb atom at H3 and the neighboring Yb atoms at T4 sites are about $2.5a_0$ and $1.5a_0$, in agreement with the measured protrusion separations in the line profile D-D′. The model of Fig. 6(d) proposes a regular arrangement with Yb atoms at T4 and H3, which gives rise to the fourfold (×4) periodicity along the Yb row. We note, however, that the ×4 segments of the ×2 rows are local and quite limited, and that no 3×4 domain was observed in this study. Therefore, we will call the Yb/Ge(111) reconstruction as the (3×2) hereafter.

In the continuous rows shown in Figs. 4(b) and 4(c), the weak twofold periodicity is found. Therefore, we assume that in these rows, the Yb atoms are adsorbed at every second T4 site. Also, the Yb atoms can fluctuate rapidly between T4 sites and the neighboring H3 sites, as shown schematically in Fig. 6(e). Such fluctuation is much faster than the STM tip motion in our measurements and thus the measured STM images reflect the time-averaged picture. For this reason, we assume that the continuous rows in STM images are due to dynamical fluctuation of the Yb atoms in ×2 rows between T4 and neighboring H3 sites. It is important that the model of Yb row shown in Fig. 6(e) suggests the donation of the appropriate number of electrons from the Yb atoms to the surface in order to stabilize the HCC structure.

Thus, the long-range ×2 ordering along the metal rows is very limited in the Yb/Ge(111)3×2 reconstruction. Most likely, this limitation explains the lack of double periodicity in LEED [Figs. 2(c) and 2(d)] and the local character of the ×2 periodicity in the filled state STM images of Fig. 3. In contrast, the 3× periodicity is clearly observed in LEED and

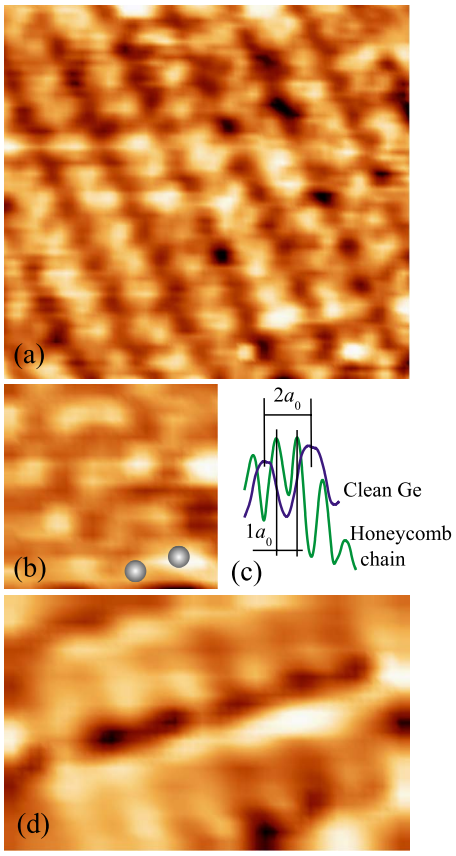

FIG. 7. (Color online) Empty state STM images at lower bias voltages. (a) V_S=+1.06 V. 7.3 nm×6.8 nm. The tunneling current is 456 pA. [(b) and (d)] V_S=+0.99 V. 2.4 nm×2.3 nm and 3.9 nm×2.5 nm, respectively. The tunneling current is 30 pA. The dimerized feature is marked in (b). (c) Corrugations of Yb/Ge(111)3×2 and clean Ge(111)$c(2\times8)$ surfaces. The line profile for Yb/Ge(111)3×2 is taken along the row of dimerized features (the honeycomb chain) in lower bias-voltage STM image.

it is well consistent with the good long-range ordering of the Yb/Ge(111)3×2 reconstruction in the perpendicular direction (i.e., across the Yb rows and Ge honeycomb chains). Moreover, the 3× LEED spots persist upon increasing the temperature up to 400 °C even, as found in Fig. 2(d), thus indicating that the HCC structure is stable at this temperature.

Figure 7(a) shows an empty state STM image measured at the relatively lower bias voltage V_S=+1.06 V. The corrugation of this image is different from those of empty state images at +2.32 V (Figs. 4 and 5) and the filled state images in Figs. 3 and 4(a). As seen in Figs. 7(b) and 7(d), high-resolution images at +1.06 V reveal rows of dimerized features. As shown in Fig. 7(c), the distance between the neighboring STM maxima along such a row (a_0) is two times smaller than the distance between the neighboring STM maxima for the Ge(111)$c(2\times8)$ surface ($2a_0$). Therefore, the structure found in Figs. 7(b) and 7(d) has the (3×1) periodicity. The building block of this structure (i.e., the dimerized feature) clearly resembles dimerlike entities caused by the Si=Si and Ge=Ge double bonds of the HCC structure in calculated empty state STM images.[6,10,15,24,32] In the case of Ge, similar features were also reported in measured empty state images for the Li/Ge(111)(3×1) (Refs. 19 and 20) and more recently the Eu/Ge(111)(3×2) (Ref. 26). Hence, we suggest that the dimerized features in the STM images of Fig. 7 are due to the Ge(b)=Ge(c) double bond on Yb/Ge(111)3×2 and that different structural elements of this reconstruction can be identified in STM images, depending on the bias voltage, namely, the Yb rows are mostly contributed at the higher bias voltage and the Ge=Ge double bonds at the lower bias voltage. Since the buckling of the Ge=Ge double bond would lead to charge redistribution between the atoms b and c, and therefore, the asymmetry of the dimerized features in STM images, we tentatively assume that no significant buckling of this bond occurs on the Yb/Ge(111)3×2. However, further investigations are required to solve this issue because the identification of tilted configuration of the double bond by STM might be complicated at RT, similar to the case of the Si dimers on the Si(100)2×1 surface.[28]

B. STS

STS was applied to gain the information about the local electronic structure of Yb/Ge(111)3×2, which was extracted from normalized conductance spectra $[(dI/dV)/(I/V)]$. Such spectra reflect the spatial variation in the local density of states and the energy positions of surface bands. However, the intensity of peaks in the spectra depends strongly on the tip-substrate configuration and the normalization procedure.[35] Numerical derivative of IV spectra acquired by CITS was applied to obtain $(dI/dV)/(I/V)$ curves using the WSXP package.[30]

Figure 8(a) shows a normalized conductance spectrum from the clean substrate. The IV curve obtained for this surface (not shown) is the result of an average over the large well-ordered $c(2\times8)$ area free of defects. In occupied orbitals (the 0 V bias voltage corresponds to the Fermi level) the curve reveals a pronounced feature at −0.80 eV and a shoulder at −0.57 eV. These states are due to the two nonequivalent rest atoms in the $c(2\times8)$ reconstruction and their energy splitting agrees well with the predicted value.[36] In unoccupied orbitals, peak at +0.61 eV and extended shoulder around 1.0 eV are present. They can be attributed to the adatom dangling-bond states.[36] The tunneling gap is found to be 0.40–0.45 eV and the valence-band maximum is located 0.17 eV below the Fermi energy, in good agreement with the results of Refs. 37 and 38, respectively.

Normalized conductance spectra for the Yb/Ge(111)-(3×2) reconstruction are represented in Figs. 8(b) and 8(c). They are taken for Yb rows and Ge honeycomb chains, respectively. For each of these spectra, the IV curve (not shown) is an average of about 20 individual spectra taken for the respective structural unit (Yb row or Ge honeycomb chain). These $(dI/dV)/(I/V)$ spectra were reproduced in several measurements. No significant difference is found for those of continuous and ×2 rows. It is intuitively understood on the basis of the similarity of the electronic structures of the HCC configurations with T4 and H3 sites, as described below. In the occupied states, the spectrum of Yb rows [Fig.

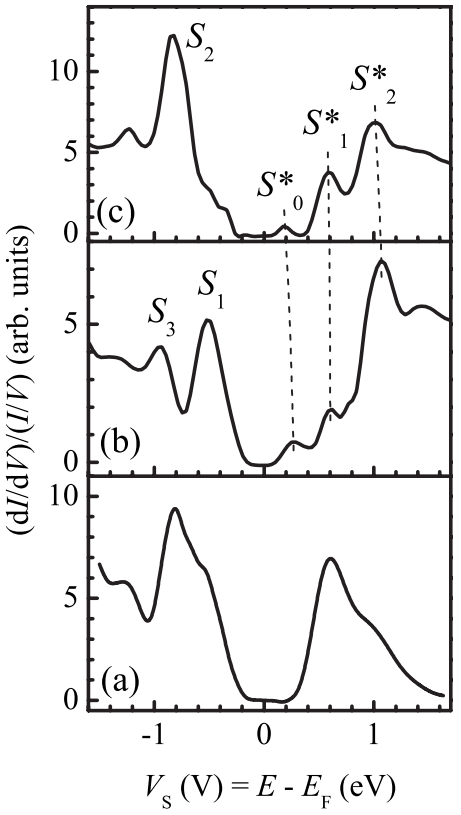

FIG. 8. Normalized conductance spectra taken from (a) the clean Ge(111)$c(2\times8)$ surface, (b) the Yb row, and (c) the Ge honeycomb chain of the Yb/Ge(111)3×2 reconstruction.

8(b)] clearly shows two features, S_1 and S_3, at −0.51 and −0.95 eV, respectively, whereas the dominant feature in the spectrum of Ge honeycomb chain [Fig. 8(c)] is a peak S_3 at −0.83 eV. In the empty states, the dominant feature of the spectrum of Yb rows is a peak S_2^* at 1.06 eV. Besides, two minor features S_0^* and S_1^* at 0.27 and 0.61 eV, respectively, are seen. In the spectrum of Ge honeycomb chain, the S_1^* and S_2^* are clearly resolved at 0.60 and 1.02 eV, respectively. The S_0^* is also found at 0.18 eV. Thus, the spectra of Yb rows and Ge honeycomb chain are rather different, allowing the identification of observed states. The tunneling gap is found to be 0.25–0.30 eV for the Yb rows and about 0.35 eV for the Ge honeycomb chain. This is consistent with photoemission data in Ref. 28, which indicate the semiconducting character of the Yb/Ge(111)3×2 reconstruction.

The band-structure calculations for the (3×2) HCC reconstruction on Ge(111) are still not reported. However, the band structure has been recently calculated for (3×1) HCC reconstructions of Tl (Ref. 39) and Li (Ref. 21) on Ge(111) as well as 3×1 and 3×2 HCC reconstructions on Si(111) (Refs. 6, 7, and 15). It is essential that the calculations in Ref. 39 were performed for two 3×1 HCC configurations, where the metal atoms are adsorbed on either H3 or T4 sites in the channels of the Ge HCC backbone (HCC-H3 and -T4 models, respectively). It has been shown that the theoretical band structure of each of the two models includes three fully occupied surface bands and two completely empty bands lying in the projected bulk band gap. For example, in the HCC-T4 model shown in Fig. 1(a) one of the three occupied bands (labeled S_a' in Ref. 39) has a bonding character between the dangling bonds of the Ge a and metal atoms. The other two bands, S_{bc}' and S_d', have a strong π bonding character between the dangling bonds of Ge atoms b and c, and a hybridized character of the dangling bond of Ge a and a back bond of Ge a with the substrate atom, respectively. The unoccupied bands (U_{bc} and U_{Tl}) have the antibonding π^* character between b and c, and mostly the metal atom and the Ge d and c, respectively. It is important that the S_{bc}' and the respective band S_{bc} in the HCC-H3 model have almost similar dispersion and binding energies, that is, the adsorption site of metal atoms in the HCC-T4 and HCC-H3 models does not affect noticeably the π bonding between the inner honeycomb atoms b and c.[39] Moreover, the differences of the dangling-bond states of the outer honeycomb atoms a and d and the unoccupied states in the HCC-H3 and T4 models are not significant. Therefore, we expect that the charge distributions (and normalized conductance spectra) for the metal rows with T4 sites (i.e., $\times2$ rows) are similar to those of T4 and H3 sites (i.e., continuous rows).

In lack of other information on the band structure of the 3×2 HCC Ge structures, we use the above theoretical data in order to discuss the possible origin of features observed for the Yb/Ge(111)3×2 in Figs. 8(b) and 8(c). The features S_1 and S_3, which are identified for the Yb rows, can be interpreted as originating from the states due to the dangling bonds of the outer Ge honeycomb atoms that surround the Yb atom (i.e., a and d). In contrast, the S_2 is identified for the Ge honeycomb chain and therefore, it is natural to assume this feature to be due to the inner Ge honeycomb atoms. It is also worth noting that the S_2 lies between the S_1 and S_3, in agreement with Ref. 39.

Above the Fermi level, the S_2^* state is a dominant one in the curve for the Yb rows. Therefore, we assume that it has an antibonding character of the bond between the Yb atoms and outer Ge honeycomb atoms. The S_1^* state, which is clearly found for the Ge honeycomb chains but not for the Yb rows, is suggested to have an antibonding character for the b and c atoms. Thus, the energy splitting of the bonding and antibonding bands for the Ge═Ge double bond in the Yb/Ge(111)3×2 reconstruction is assumed to be 1.43 eV. It is important that the above interpretation of S_1^* and S_2^* agrees with STM observations. That is, the Yb atoms clearly contribute to STM images at higher bias voltages (typically at 2.0–2.3 V) and the inner Ge honeycomb atoms contribute to those of lower bias voltages (typically about 1.0 V). It is more difficult to interpret the S_0^* state. No additional unoccupied band was found in calculations for the (3×1) HCC structure. However, the (3×2) HCC structure involves the additional honeycomb atom [i.e., a' in the HCC-T4 of Fig. 1(b) and d' in the HCC-H3 of Fig. 1(c)] that does not interact with the metal atoms and can be the origin of S_0^*. Band-structure calculations performed for the (3×2) HCC structure are required to solve the origin of this feature in more detail.

IV. CONCLUSION

The Yb/Ge(111)3×2 reconstruction with the metal coverage of 1/6 ML has been studied by STM and STS. The

STM images are found to be dependent on bias polarity and voltage. In the filled states, STM images show the zigzag chain features which are consistent with the HCC structure. They demonstrate the basic (3×1) periodicity with a local pairing of protrusions. The brightness contrast of the adjacent rows of the zigzag chains is pronounced at $V_S=-1.08$ V, giving evidence for the nonequivalence of the outer Ge honeycomb chain atoms. The empty state images at the higher bias voltage ($V_S=2.0-2.3$ V) show the single rows of protrusions which are assumed to be due to the Yb atoms. The similar adsorption sites are found for the Yb atoms in the well-defined $\times2$ rows. However, the Yb rows can locally be distorted and show the $\times4$ periodicity, where the Yb atoms are adsorbed on two different sites that are well consistent with the T4 and H3 sites. Also, the dynamical fluctuation of Yb atoms between the neighboring T4 and H3 sites is assumed to account for the continuous rows observed locally in STM images. The point defects found in the Yb rows change the local density of Yb atoms and, therefore, the local number of electrons donated from the metal atoms to the surface. This leads to an appearing of depressions on one of the adjacent rows of zigzag chain features in the filled state STM images, thus affecting the Ge honeycomb chain. The empty state STM images taken at the lower bias voltage (about 1.0 V) demonstrate the rows of dimerized features which are interpreted as originating from the Ge(b)=Ge(c) double bond. Such rows have the (3×1) periodicity. Thus, on the basis of the STM results, the Yb/Ge(111)3×2 reconstruction does not exhibit an extended long-range $\times2$ ordering at room temperature, which reasonably explains the lack of half-order periodicity for this surface in LEED.

The normalized conductance spectra of Yb/Ge(111)3×2 show the tunneling gap (about 0.3 V), in agreement with the semiconducting character of this surface found by valence-band photoemission in Ref. 28. They allow the identification of three features lying 0.51 (S_1), 0.83 (S_2), and 0.95 eV (S_3) below the Fermi energy and three features lying about 0.2 (S_0^*), 0.60 (S_1^*), and 1.06 eV (S_2^*) above the Fermi energy. The S_2 and S_1^* are assumed to be due to the double bond between the inner Ge atoms of the honeycomb chain (i.e., the atoms b and c) and have the π bonding and π^* antibonding character between the dangling bonds of these atoms, respectively. This infers the energy splitting of 1.43 eV between the bonding and antibonding bands for the Ge=Ge double bond. The S_1 and S_3 are assumed to be due to the outer Ge honeycomb atoms. The S_2^* is interpreted to have the antibonding character between the Yb atoms and outer Ge honeycomb atoms. The origin of S_0^* has remained so far unclear; it may originate from the outer Ge honeycomb atoms that do not interact with the Yb atoms in the (3×2) HCC structure directly.

ACKNOWLEDGMENTS

The authors are grateful to H. Ollila for the technical assistance. This work has been supported by the Academy of Finland (Grants No. 122743 and No. 122355) and Finnish Academy of Sciences and Letters. The Carl Tryggers Foundation (M.P.J.P.), the Turku University Foundation (M.P.J.P.), and the Emil Aaltonen Foundation (M.P.J.P.) are acknowledged for financial support.

*Corresponding author; m.kuzmin@mail.ioffe.ru

[1] V. G. Lifshits, A. A. Saranin, and A. V. Zotov, *Surface Phases on Silicon* (Wiley, Chichester, 1994), p. 450.
[2] K. J. Wan, X. F. Lin, and J. Nogami, Phys. Rev. B **46**, 13635 (1992); **47**, 13700 (1993).
[3] T. Okuda, H. Shigeoka, H. Daimon, S. Suga, T. Kinoshita, and A. Kakizaki, Surf. Sci. **321**, 105 (1994); H. H. Weitering, X. Shi, and S. C. Erwin, Phys. Rev. B **54**, 10585 (1996).
[4] C. Collazo-Davila, D. Grozea, and L. D. Marks, Phys. Rev. Lett. **80**, 1678 (1998).
[5] L. Lottermoser, E. Landemark, D.-M. Smilgies, M. Nielsen, R. Feidenhans'l, G. Falkenberg, R. L. Johnson, M. Gierer, A. P. Seitsonen, H. Kleine, H. Bludau, H. Over, S. K. Kim, and F. Jona, Phys. Rev. Lett. **80**, 3980 (1998).
[6] S. C. Erwin and H. H. Weitering, Phys. Rev. Lett. **81**, 2296 (1998).
[7] M.-H. Kang, J.-H. Kang, and S. Jeong, Phys. Rev. B **58**, R13359 (1998).
[8] G. Lee, S. Hong, H. Kim, D. Shin, J.-Y. Koo, H.-I. Lee, and Dae Won Moon, Phys. Rev. Lett. **87**, 056104 (2001).
[9] G. Lee, S. Hong, H. Kim, and J.-Y. Koo, Phys. Rev. B **68**, 115314 (2003).
[10] F. Palmino, E. Ehret, L. Mansour, J.-C. Labrune, G. Lee, H. Kim, and J.-M. Themlin, Phys. Rev. B **67**, 195413 (2003).
[11] E. Ehret, F. Palmino, L. Mansour, E. Duverger, and J.-C. Labrune, Surf. Sci. **569**, 23 (2004).
[12] M. Kuzmin, R.-L. Vaara, P. Laukkanen, R. E. Perälä, and I. J. Väyrynen, Surf. Sci. **538**, 124 (2003); **549**, 183 (2004).
[13] M. Kuzmin, P. Laukkanen, R. E. Perälä, R.-L. Vaara, and I. J. Väyrynen, Phys. Rev. B **71**, 155334 (2005).
[14] K. Sakamoto, A. Pick, and R. I. G. Uhrberg, Phys. Rev. B **72**, 045310 (2005); **72**, 195342 (2005).
[15] R. H. Miwa, Phys. Rev. B **72**, 085325 (2005).
[16] C. Battaglia, H. Cercellier, C. Monney, L. Despont, M. G. Garnier, and P. Aebi, J. Phys.: Conf. Ser. **100**, 052078 (2008).
[17] C. Battaglia, P. Aebi, and S. C. Erwin, Phys. Rev. B **78**, 075409 (2008).
[18] C. Battaglia, H. Cercellier, C. Monney, M. G. Garnier, and P. Aebi, EPL **77**, 36003 (2007).
[19] G. Lee, J. Kim, H. Mai, I. Chizhov, and R. F. Willis, J. Vac. Sci. Technol. A **18**, 1488 (2000).
[20] G. Lee, H. Mai, and R. F. Willis, Phys. Rev. B **63**, 085323 (2001).
[21] M. Gurnett, L. J. Holleboom, H. M. Zhang, and L. S. O. Johansson, Surf. Sci. **603**, 727 (2009).
[22] G. Lee, H. Cho, Y. Kim, and H. Shim, J. Phys. Soc. Jpn. **76**, 044704 (2007).
[23] D. Grozea, E. Bengu, C. Collazo-Davila, and L. D. Marks, Surf.

Rev. Lett. **6**, 1061 (1999).
[24] J. Y. Lee and M.-H. Kang, Phys. Rev. B **66**, 233301 (2002).
[25] G. Lee, J. Kim, I. Chizhov, H. Mai, and R. F. Willis, Phys. Rev. B **61**, 9921 (2000); M. Yoon, H. Mai, G. Lee, and R. F. Willis, Surf. Sci. **463**, 183 (2000).
[26] M. Kuzmin, P. Laukkanen, R. E. Perälä, and I. J. Väyrynen, Phys. Rev. B **73**, 125332 (2006).
[27] M. Kuzmin, R. E. Perälä, P. Laukkanen, M. Ahola-Tuomi, and I. J. Väyrynen, Phys. Rev. B **74**, 115320 (2006).
[28] M. Kuzmin, K. Schulte, P. Laukkanen, M. Ahola-Tuomi, R. E. Perälä, M. Adell, T. Balasubramanian, and I. J. Väyrynen, Phys. Rev. B **75**, 165305 (2007).
[29] C. Wigren, J. N. Andersen, R. Nyholm, U. O. Karlsson, J. Nogami, A. A. Baski, and C. F. Quate, Phys. Rev. B **47**, 9663 (1993); C. Wigren, J. N. Andersen, R. Nyholm, M. Göthelid, M. Hammar, C. Törnevik, and U. O. Karlsson, *ibid.* **48**, 11014 (1993); R.-L. Vaara, M. Kuzmin, R. E. Perälä, P. Laukkanen, and I. J. Väyrynen, Surf. Sci. **529**, L229 (2003); **539**, 72 (2003); R.-L. Vaara, M. Kuzmin, P. Laukkanen, R. E. Perälä, and I. J. Väyrynen, Appl. Surf. Sci. **220**, 327 (2003).
[30] I. Horcas, R. Fernandez, J. M. Gomez-Rodriguez, J. Colchero, J. Gomez-Herrrero, and A. M. Baro, Rev. Sci. Instrum. **78**, 013705 (2007).
[31] T. Sekiguchi, F. Shimokoshi, T. Nagao, and S. Hasegawa, Surf. Sci. **493**, 148 (2001).
[32] S. Hong, G. Lee, and H. Kim, J. Korean Phys. Soc. **47**, 100 (2005); Surf. Sci. **600**, 3606 (2006).
[33] K.-D. Ryang, P. G. Kang, H. W. Yeom, and S. Jeong, Phys. Rev. B **76**, 205325 (2007).
[34] S. C. Erwin, I. Barke, and F. J. Himpsel, Phys. Rev. B **80**, 155409 (2009).
[35] J. Tersoff and D. R. Hamann, Phys. Rev. Lett. **50**, 1998 (1983); Phys. Rev. B **31**, 805 (1985); Z.-C. Dong, D. Fujita, and H. Nejoh, *ibid.* **63**, 115402 (2001).
[36] N. Takeuchi, A. Selloni, and E. Tosatti, Phys. Rev. Lett. **69**, 648 (1992).
[37] R. M. Feenstra, S. Gaan, G. Meyer, and K. H. Rieder, Phys. Rev. B **71**, 125316 (2005).
[38] G. M. Guichar, G. A. Garry, and C. A. Sébenne, Surf. Sci. **85**, 326 (1979).
[39] S. Hatta, T. Aruga, C. Kato, S. Takahashi, H. Okuyama, A. Harasawa, T. Okuda, and T. Kinoshita, Phys. Rev. B **77**, 245436 (2008).